Guided Wave Based-Occupancy Grid Robotic Mapping

Morteza Tabatabaeipour[1], Oksana Trushkevych[2], Gordon Dobie[1], Rachel S. Edwards[2], Charles Macleod[1], Stephen G. Pierce[1]

[1] Centre for Ultrasonic Engineering, Department of Electronic and Electrical Engineering, University of Strathclyde, Glasgow G11XW, UK
[2] Department of Physics, University of Warwick, Coventry CV4 7AL, UK
morteza.tabatabaeipour@strath.ac.uk

Abstract. Asset inspection of large structures such as storage tanks in the oil, gas and petrochemical industry is challenging, either requiring labour-intensive manual measurements or using robotic deployment to make the measurements. Current robotic systems employ point-by-point scanning, which is time-consuming. Using guided waves for such inspections is attractive as they provide a mechanism for monitoring the inaccessible areas and simultaneously providing structural location data to speed up the inspection process. In this research, shear horizontal (SH) guided waves generated by electromagnetic acoustic transducers (EMATs) are used to screen a large area using a crawler. EMATs with 22 mm wavelength are used to generate the first two SH modes: a non-dispersive SH0 and highly dispersive SH1 on a 10 mm thick steel sample. Previously, we have demonstrated the feasibility of guided wave-based occupancy grid mapping (GW-OGM) for mapping a structure's edges. In this work, the GW-OGM technique is generalised to identify and estimate the location of a flat bottom hole in a pitch-catch mode. The simulation and empirical data demonstrate that the location of damage can be identified as the robot navigates on the component, with full coverage. Moreover, the simulated data are in good agreement with the experimental results on the generation of SH wave modes.

Keywords: Bayesian imaging, Guided waves, Occupancy grid mapping, Shear horizontal (SH) waves.

1 Introduction

Large structural assets, such as storage tankers and large-bore above-ground pipework, used in the energy industries are an extremely important part in the dynamic system of providing power across a given country [1]. In order for these structures to remain in use they have to be rigorously checked and maintained to meet high safety standards. Inspection of these assets can be resource consuming for a business due to the required manpower for the task, costly specialized equipment to carry out the procedure, lengthy inspection processes and the cost of the downtime of the component being inspected.

Portable and semi-automated inspection scanners were developed to reduce inspection time and the risk to operators. This was then followed up by new robotic inspection systems giving more manoeuvrability and increased automation capabilities [2][3][4]. The Eddyfi and Sonasearch crawlers, equipped with dry coupled ultrasonic transducers and phased array wheel probes respectively, are two examples of point-by-point inspection crawlers that were designed to measure the thickness of storage tanks [4], [5]. Although the crawler reduces the time of the inspection procedure through partial automation, it is still time consuming due to the nature of point inspection, as well as its inability to measure certain geometries and inaccessibly regions, meaning a full mapping of a structure cannot be obtained easily or as quickly as needed.

Ultrasonic guided waves have received much attention in recent years for the ultrasonic evaluation of various materials and structures [6]. Significant advances have been made in utilising guided waves for detection of defects within large structures, and have successfully demonstrated broad applications for the screening of many types of industrial structures [7], [8] with particular success on pipework [9]. This is being followed by attempts to construct guided wave-based structural images such as the reconstruction algorithm for probabilistic inspection of damage (RAPID), which is currently being investigated for localising damage in structures [10], [11].

Despite the usage of appropriate sensors for mobile robotic inspection, environmental identification and mapping of surrounding regions using a mobile robot is also an essential task for a crawler robot if is to be an autonomous intelligent vehicle. Many tasks such as localisation, navigation, collision avoidance and path planning are subject to a well-defined mapping of the environment [12][13]. External surroundings are currently mapped with range finder technologies [13]. However, the internal features (edges, welded joints, defects) of a component are also important to be mapped so that previously unreachable features can be inspected, as well as determining if further close-up inspections are needed for examining certain areas. This is also important for influencing the path planning of the robotic inspection and/or an autonomous inspection.

Occupancy grid mapping (OGM) is a well-established technique in robotics that is currently used for estimating a map of an unknown urban environment, typically using a light detection and ranging (LiDAR) sensor [13]. A successful feasibility study on incorporating guided waves into OGM was carried out in a pseudo-pulse echo mode by the authors to map the edges of an inspected component, see Fig. 1. It was shown that guided wave-based OGM can estimate the map of a component with the identification of its boundaries, with more detail given in [14]. However, to make a comprehensive mapping to include defects as well, it is necessary to extend this OGM technique for a pitch-catch measurement mode.

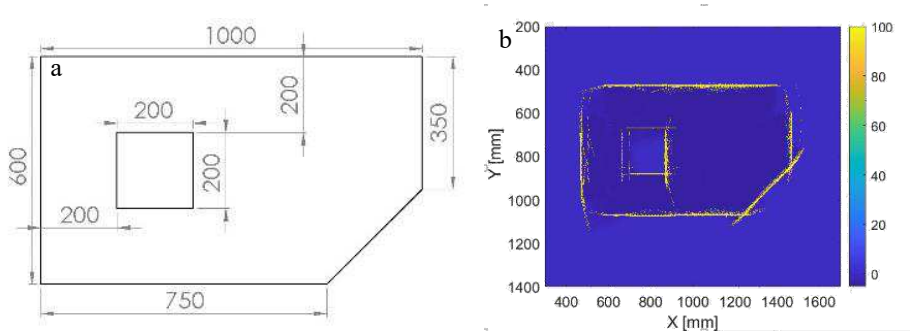

Fig. 1. Guided wave-based occupancy grid mapping for the identification of boundaries, a) simulated 10 mm thick steel sample, units are in mm, b) guided wave-based OGM results; the yellow points indicate the edges of the simulated sample (a), [14]

In this paper, the OGM is further evaluated for identification of defects using shear horizontal (SH) guided waves. The integrated inspection system can be used to autonomously identify the geometrical features of industrial infrastructures in the future. As a result, this research paves the way for further investigations on the next generation of autonomous ultrasonic mobile inspection systems, in order to reduce the inspection time.

2 Finite Element Analysis

A miniaturized EMAT with 22 mm wavelength was simulated on a 10 mm thick steel sample in the OnScale software, as shown in Fig. 2. Details on the EMAT model can be found in [15]. The EMATs used for experiments had varied designs; design 2 was used for generation and design 3 for detection, with full details given in [16]. With a prior experimental knowledge [16], a separation distance of 300 mm was used for a pitch-catch measurement to identify the damage positions. A 3-cycle tone burst at a centre frequency of 200 kHz was fed into the EMAT to generate SH wave modes. Signals were further monitored to validate the simulation and identify the available wave modes. Fig. 3 illustrates that both non-dispersive SH0 and dispersive SH1 have been generated at this frequency. Furthermore, it also shows that the SH1 wave mode has more interaction with a 40 mm diameter flat bottom hole (FBH) with a 5 mm depth modelled in the sample compared to the SH0 wave mode, see Fig. 3c.

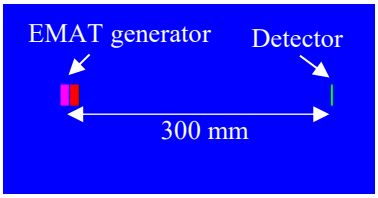

Fig. 2. Guided wave set-up in a pitch-catch mode modelled in OnScale

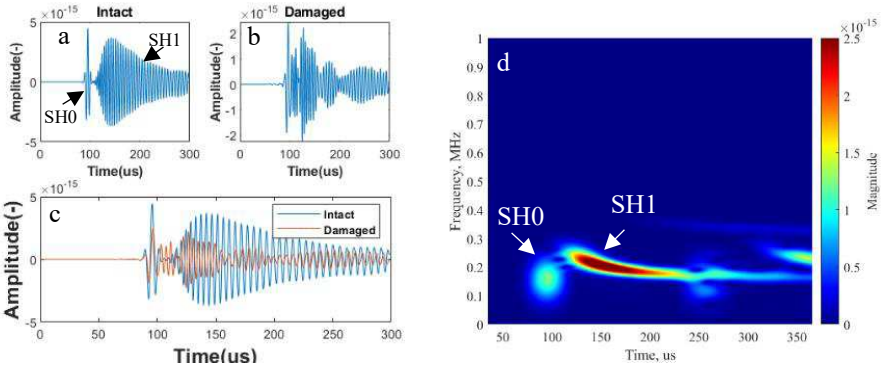

Fig. 3. Signals measured in simulation, a) raw signal captured at intact region, b) damaged path, c) overlaid for a fair comparison, d) Short-time Fourier transform (STFT) of the simulated intact signal

2.1 Signal processing

Having validated the simulation, multiple points on the sample for scans along two orthogonal lines were monitored, resembling a crawler navigating and capturing the EMAT data. The trajectory is shown in Fig. 4a. A signal from the intact part of the sample was selected as a reference to calculate the Pearson correlation coefficient (PCC) as:

$$PCC_t = \frac{cov(S_t, S_r)}{\sigma_t \sigma_r}, \tag{1}$$

where S_t and σ_t are measured signals at a specific time step and its standard deviation, and S_r and σ_r are the reference signal and its standard deviation, respectively [17], [18]. It is important to mention that cov represents the covariance of the aforementioned signals and the t subscript for the PPC indicates the measurement time step. The signal difference coefficient (SDC) in each time step can, therefore, be expressed as Eq. (1),

$$z_t = (1 - PCC_t)^2. \tag{2}$$

To show how the z_t feature behaves, monitored points across the horizontal line (see Fig. 4a) were evaluated. Fig. 4b demonstrates that there exists a significant difference between the signals measured in the vicinity of a defect and the reference signal. Note that the FBH was modelled on the back side of the sample.

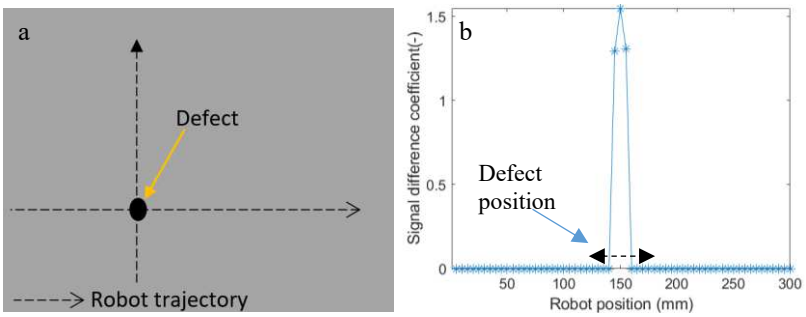

Fig. 4. a) Robot trajectory on the sample, b) signal difference coefficient measured as the crawler navigates across the sample on the horizontal line

2.2 Mapping Algorithm

Occupancy grid mapping is exploited in this section to evaluate the robotic mapping in the pitch-catch mode. OGM represents a map of the environment as an evenly spaced field of grid cells (random variables) each representing the probability of the occupancy of that cell OGM estimates the posterior probability over all grid cells of the map given the data. The log-odd representation of OGM is formulated as Eq. (2), [19],

$$l(m_{x,y}|z_{1:t}, x_{1:t}) = l(m_{x,y}|z_t, x_t) + l(m_{x,y}|z_{1:t-1}, x_{1:t-1}) - l(m_{x,y}) \quad (3)$$

where $l(m_{x,y}|z_t, x_t)$, $l(m_{x,y}|z_{1:t-1}, x_{1:t-1})$ and $l(m_{x,y})$ are the inverse sensor model, recursive term and the prior map respectively. $m_{x,y}$, $z_{1:t}$ and $x_{1:t}$ are a vector of grid cells, the set of measurements up to time step t and the set of all robot positions respectively.

The inverse sensor model is formulated as shown in Table 1. This approximate sensor model was inspired by the RAPID algorithm [20], [21]. A detailed investigation of an exact sensor model for EMAT transducers in a pitch-catch mode is out of the scope of this paper but is currently under consideration; this approximate model is suitable to assess its applicability. Fig. 5 illustrates the implemented OGM on the simulated data at three different time steps as the robot navigates the path shown in Fig. 4a. As soon as the robot passes the defect on the horizontal line, the damaged path stands out, see Fig. 5b. In order to determine the exact location of the defect, the robot should navigate along two paths, with the optimal the crossed paths shown here, to assign a higher likelihood to the damage location compared to the other parts of the damaged path, as shown in Fig. 5c. The future work will focus on determining the minimum wall thickness as well as the damage position.

Table 1. Inverse sensor model for the pitch-catch measurement

1: **Algorithm inverse_sensor_model** $(m_{x,y}, x_t, z_t, d, \beta)$:
2: (x_i, y_i) are the centre of $m_{x,y}$
3: (x_T, y_T), (x_R, y_R) and d are the EMAT transmitter position, EMAT receiver position and the separation distance, respectively
4: $R_{x,y} = \frac{\sqrt{(x_T-x_i)^2+(y_T-y_i)^2}+\sqrt{(x_R-x_i)^2+(y_R-y_i)^2}}{d}$
5: if $\beta > R_{x,y}$
6: return $\{ z_t * \frac{\beta-R_{x,y}}{\beta-1} \}$
7: if $\beta \leq R_{x,y}$
8: return $\{ 0 \}$
9: endif

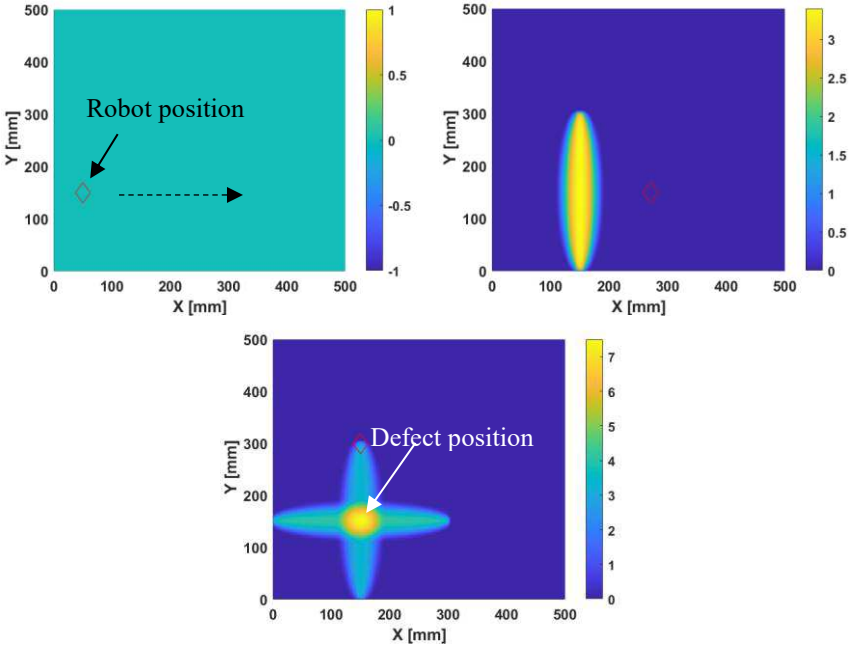

Fig. 5. Guided wave-based occupancy grid mapping in the pitch-catch mode at three different time steps, t_{10}, t_{60}, t_{120}, note that the red diamond indicates the robot position. Images are in linear scale

3 Experimental Analysis

SH0 and SH1 guided wave modes were generated on a 10 mm mild steel sample using miniaturised EMATs [16]. Miniature EMATs were used because they can be mounted on an Inuktun Micro-Tracks platform. In the current work, however, the scanning was

done manually. A RITEC pulser/receiver was used to drive EMAT generation at 200 kHz, and detection was done with a second miniaturised EMAT, amplified by 60dB and measured using a Tektronix DPO2024B oscilloscope.
Fig. 6 demonstrates the measured signals for intact and damaged paths. Experimental signals are in very good agreement with the simulation data shown in Fig. 3c. Using Eq. (3), a signal difference coefficient (SDC) of 0.84 was calculated between these empirical signals, showing the high sensitivity of the SDC feature to the defects. Furthermore, the sample was scanned across a single line only, and the corresponding SDC values were calculated and are shown in Fig. 7a. As expected, the defect region with the highest SDC is visible; consequently, the GW-OGM shows the damaged path as the crawler approaches it, see Fig. 7b.

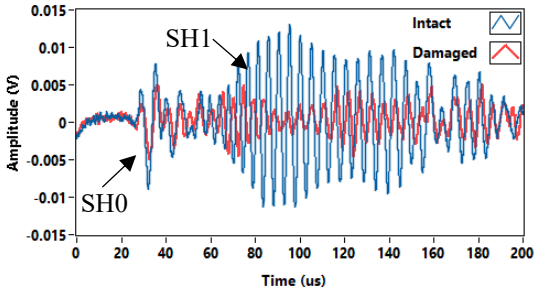

Fig. 6. Experimental signals measured in the pitch-catch mode

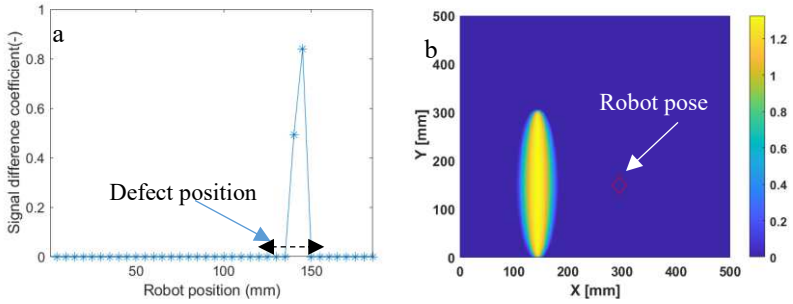

Fig. 7. Experimental results a) Signal difference coefficient, b) GW-OGM in a pitch-catch mode at t_{38}

4 Conclusions

A pitch-catch measurement was incorporated into the OGM algorithm to estimate the position of the defects as the robot navigates the sample. The algorithm was applied to analyse simulation and experimental data in pitch-catch mode. As a result, it was shown that the proposed OGM has a high potential to be extended to include both detection of defects and the sample boundaries all together. More experiments are needed to

investigate the practical issues that may arise during the inspection process, and confirm implementation onto the robotic platform, see Fig. 8. Future work will focus on the fusion of both pulse-echo and pitch-catch methods into a holistic GW-OGM technique, in order to pave the way towards the next generation of autonomous inspection systems using guided waves.

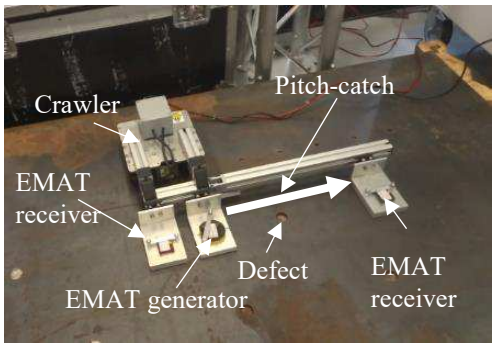

Fig. 8. Mobile robot equipped with the miniaturized EMATs for both pitch-catch and pseudo-pulse echo measurements

5 Acknowledgments

This work was supported by EPSRC "Delivering Enhanced Through-Life Nuclear Asset Management" (EP/R004889/1), Advanced Nuclear Research Centre (ANRC) and EPSRC "UK Research Centre in Non-Destructive Evaluation (RCNDE)" (EP/L022125/1).

6 References

[1] 'https://www.loc.gov/rr/business/BERA/issue5/transportation.html', *Accessed May 2020*. .

[2] P. G. Backes, Y. Bar-Cohen, and B. Joffe, 'Multifunction Automated Crawling System (MACS)', *Proc. - IEEE Int. Conf. Robot. Autom.*, vol. 1, no. April, pp. 335–340, 1997.

[3] A. Kroll, 'A survey on mobile robots for industrial Inspections', *Intell. Auton. Syst. 10 IAS 2008*, pp. 406–414, 2008, doi: 10.3233/978-1-58603-887-8-406.

[4] S. Walker and S. Rubin, 'Integrity Testing of Storage Tank Structure Using Robotic Ultrasound', US 2020/0054379 A1, 2020.

[5] 'https://www.silverwingndt.com/scorpion2/', *Accessed Jan*, 2020. .

[6] P. Cawley, 'Practical guided wave inspection and applications to structural health monitoring', presented at the 5th Australasian Congress on Applied Mechanics (ACAM 2007), Brisbane, Australia, Dec. 2007.

[7] P. Cawley, 'Practical guided wave inspection and applications to structural health monitoring', p. 10.

[8] K. Yang, J. A. Rongong, and K. Worden, 'Damage detection in a laboratory wind turbine blade using techniques of ultrasonic NDT and SHM', *Strain*, vol. 54, no. 6, p. e12290, Dec. 2018, doi: 10.1111/str.12290.

[9] A. Demma and D. Alleyne, 'Corrosion monitoring of buried piping systems within nuclear installations', *Corros. Eng. Sci. Technol.*, vol. 47, no. 7, pp. 484–488, Nov. 2012, doi: 10.1179/1743278212Y.0000000022.

[10] E. Monaco *et al.*, 'Methodologies for guided wave-based SHM system implementation on composite wing panels: results and perspectives from SARISTU scenario 5', in *Smart Intelligent Aircraft Structures (SARISTU)*, Springer, Cham, 2016, pp. 495–527.

[11] M. Tabatabaeipour, J. Hettler, S. Delrue, and K. V. D. Abeele, 'Visualization of delaminations in composite structures using a baseline-free, sparse array imaging technique based on nonlinear lamb wave propagation', *Acta Acust. United Acust.*, vol. 103, no. 6, 2017, doi: 10.3813/AAA.919128.

[12] D. M. Varisco, G. Badawi, and S. Athar, 'Learning Occupancy Grid Maps with Forward Sensor Models', vol. 43, no. 1998, pp. 111–127, 2003, doi: 10.1023/A:1025584807625.

[13] E. Kaufman, K. Takami, T. Lee, and Z. Ai, 'Autonomous Exploration with Exact Inverse Sensor Models', *J. Intell. Robot. Syst. Theory Appl.*, vol. 92, no. 3–4, pp. 435–452, 2018, doi: 10.1007/s10846-017-0710-7.

[14] M. Tabatabaeipour *et al.*, 'A Feasibility Study on Guided Wave- Based Robotic Mapping', *IEEE Int. Ultrason. Symp. IUS*, vol. 2019-Octob, pp. 1567–1570, 2019, doi: 10.1109/ULTSYM.2019.8926029.

[15] P. A. Petcher and S. Dixon, 'Mode mixing in shear horizontal ultrasonic guided waves', *Nondestruct. Test. Eval.*, vol. 9759, pp. 1–20, 2017, doi: 10.1080/10589759.2016.1184268.

[16] O. Trushkevych *et al.*, 'Miniaturised SH EMATs for fast robotic screening of wall thinning in steel plates', *IEEE Sens. J. Rev.*, 2020.

[17] T. P. Hettmansperger and J. W. McKean, 'Correlation and Covariance', in *Robust and Nonparametric Statistical Methods*, 2ed ed., CRC Press.

[18] J. Hettler, M. Tabatabaeipour, S. Delrue, and K. Van Den Abeele, 'Linear and nonlinear Guided Wave imaging of impact damage in CFRP using a probabilistic approach', *Materials*, vol. 9, no. 11, 2016, doi: 10.3390/ma9110901.

[19] S. Thrun, W. Burgard, and D. Fox, *Probabilistic robotics*. The MIT Press, 2006.

[20] J. L. Rose, *Ultrasonic Guided Waves in Solid Media*. Cambridge University Press, 2014.

[21] M. Tabatabaeipour, J. Hettler, S. Delrue, and K. Van Den Abeele, 'Reconstruction Algorithm for Probabilistic Inspection of Damage (RAPID) in Composites', presented at the 11th European Conference on Non-Destructive Testing (ECNDT 2014), Prague, Czech Republic, Oct. 2014.